Published in final edited form as:
J Neurosci. 2010 November 24; 30(47): 15962–15968. doi:10.1523/JNEUROSCI.4047-10.2010.

Permeability of the Paranodal Junction of Myelinated Nerve Fibers

A. Mierzwa, **S. Shroff**, and **J. Rosenbluth***
Dept. Physiology & Neuroscience and Rusk Institute, N.Y.U. School of Medicine, New York, NY 10016, USA.

Abstract

We have used fluorescent dextran tracers to test the 'tightness' of the paranodal junction of living or fixed myelinated fibers in mouse sciatic nerve. Both 3000 and 70,000 MW tracers are able to penetrate from the perinodal space symmetrically into the paranodes on either side of the node of Ranvier at a rate consistent with diffusion through an elongated helical pathway between the paranodal 'terminal loops' of the myelin sheath. This pathway thus provides an access route for movement of water soluble nutrients and metabolites to and from the internodal axon and constitutes a pathway through which juxtaparanodal potassium channels may be activated and may in turn affect nodal excitability. This pathway may also allow access of antibodies and toxic molecules to the internodal axon in paraneoplastic syndromes and demyelinating diseases.

Keywords

saltatory conduction; node of Ranvier; axoglial junction; Schmidt-Lanterman cleft; juxtaparanode; potassium channels; myelin

Introduction

Early diagrams of myelinated nerve fibers depicted myelin as a tight-fitting lipidic sleeve around the axon, interrupted periodically at nodes of Ranvier (Huxley and Staempfli, 1949). This architecture appeared not only to ‘insulate’ the covered axon, but also to prevent short circuiting of nodal action currents under the myelin sheath (Tasaki, 1939). Later studies showed that compact myelin is in fact separated from the axon by a 10nm ‘periaxonal space’ (Robertson, 1959) except at the paranodal junction (PNJ) flanking each node. There the space narrows to ~2–4nm and is traversed by ‘transverse bands’, intercellular ridge-like structures that extend between the terminating myelin lamellae and the axolemma (reviewed by Rosenbluth, 2009).

The presence of a periaxonal space within the PNJ raises questions about the permeability of the junction. The extent to which the PNJ permits longitudinal current flow has been a subject of interest, particularly in view of the accumulations of fast, voltage-gated K+ channels in the juxtaparanodal (JP) region of the axolemma under the myelin sheath just beyond the paranode (Wang et al., 1993). Can nodal action currents activate these K+ channels? If so, to what extent does their activity affect nodal properties? In view of the high lipid content of compact myelin, additional questions arise about access of the internodal axon to nutrients and other water-soluble molecules (Rosenbluth, 2009).

*Corresponding author: Dr. J. Rosenbluth, Dept. Physiology, NYU School of Medicine, 550 First Avenue, PHB 833, New York, NY 10016, Phone: 212-263-6326, rosenj03@med.nyu.edu.

Previous tracer studies of CNS myelinated fibers showed penetration of colloidal lanthanum into the paranodal junctional cleft (Hirano and Dembitzer, 1969) and microperoxidase reaction product in the internodal periaxonal space (Feder, 1971), suggesting the presence of patent channels through the paranode. In contrast, early electrophysiological studies showed that K+ channel blocking agents had no significant effect on conduction by normal living PNS nerve fibers (Chiu and Ritchie, 1980; Sherratt et al., 1980), implying lack of conductive pathways between juxtaparanodal K+ channels and the node of Ranvier. Equivalent results were obtained with CNS myelinated fibers (Kocsis and Waxman, 1980). Only after manipulation of the fibers, resulting in 'exposure' of the juxtaparanodal K+ channels, did K + channel block have an effect (Brismar, 1981). More recent in vitro studies, however, have shown that 4-AP (Vabnick et al, 1999) and peptide K+ channel blockers (Devaux and Gow, 2008) do modify conduction in small-caliber CNS myelinated fibers.

Based on these disparate results, it is not clear to what extent the PNJ of normal living nerve fibers in vivo is penetrable and to what extent it constitutes a pathway for current flow to and from JP K+ channels and for molecular traffic between the perinodal extracellular space and the internodal periaxonal space.

In order to assess the 'tightness' of the PNJ in both living and fixed PNS nerve fibers and the extent to which the juxtaparanodal and internodal periaxonal spaces can be accessed through it, we have followed the movement of fluorescent dextran tracers that are relatively inert and non-toxic. These tracers can be applied to nerves in vivo or in vitro, and their location within individual nerve fibers determined readily by epifluorescence microscopy.

Materials & Methods

Live nerves

All animal procedures were carried out in accordance with protocols approved by the NYU School of Medicine Institutional Animal Care and Use Committee.

Dextrans (Invitrogen) of molecular weight 3000 ('3K') and 70,000 ('70K') coupled to either fluorescein (FITC) or rhodamine B (RB) were reconstituted in 1X tris-buffered saline (TBS) (3K-FITC to 10mg/ml; 70K-RB to 25mg/ml), aliquotted and stored at −80°C. The 3K dextran used has an estimated diameter of 2.6nm, and the 70K dextran has an estimated diameter of 12–16nm (Sykova and Nicholson, 2008). At the time of use aliquots were thawed, mixed together and diluted ~1:5 in 1X TBS.

Male or female mice were anesthetized with pentobarbital, and the sciatic nerves exposed in the thigh region. ~10μL of the diluted dextrans was injected into each nerve via a Hamilton syringe and 30 gauge needle, resulting in some swelling and coloration of the nerve over a length of ~1–2cm. After injection, the muscles were approximated, the nerve was kept moist, and the animal maintained under anesthesia in a warm chamber for time periods ranging from 0 to 4hr. At the end of that time, the animal was fixed by transcardiac perfusion of 4% buffered formaldehyde, freshly made up from paraformaldehyde. The injected nerve was simultaneously flooded with fixative and left in situ.

After fixation, the nerve was excised, rinsed 6 × 1min in 1X TBS and then teased on a subbed slide with two 31-gauge syringe needles. Teased fibers were mounted in an anti-fade medium (Vectashield), coverslipped and examined immediately in an inverted Hoffman interference contrast microscope equipped for epifluorescence microscopy. Total times of exposure to tracer are expressed in minutes as the "live" time plus the "processing" time; e.g. 90 (60+30).

The teased fibers were surveyed by Hoffman interference contrast microscopy for nodes of Ranvier, appearing as circumferential constrictions in the cylindrical fibers, and those regions were then examined by fluorescence microscopy using filter cubes that provided excitation wave lengths appropriate for FITC-3K dextran and RB-labeled 70K dextran respectively. Fluorescent fibers were photographed through 40× or 100× objective lenses, and the Hoffman and fluorescence images were then superimposed. Some fibers were examined by confocal microscopy, and image stacks of longitudinally oriented fibers were rotated to provide end on views.

Fixed nerves

Mice were anesthetized as above and the sciatic nerves exposed. The epineurium was incised longitudinally in situ with the tip of a 31 gauge needle, and the nerve was then excised, immersed in buffered 3%glutaraldehyde/2%formaldehyde for 2d, then rinsed and stored in 1X TBS for up to 1wk. These nerves were then covered with dextran solutions for ½ –4hr, rinsed, teased, mounted and examined by Hoffman and epifluorescence microscopy or confocal microscopy to follow tracer penetration in sciatic nerve fibers after fixation. In this paradigm, the time from rinsing to photography of the fluorescent images was approximately 15min, and tracer movement during that time is included in the measurements and calculations (e.g., 135min = 120 + 15). All measurements were made on nodes remote from the cut ends of the nerves to exclude tracer entering the fibers through that route.

Measurements of tracer spread

Fluorescence photomicrographs were analyzed using ImageJ software (NIH) to determine the overall extent of longitudinal tracer movement in both directions from each nodal slit. Total spread on both sides was measured, and 0.75μm subtracted to allow for tracer within the nodal gap. The remainder was divided by 2 to obtain average spread into each myelin segment.

The experiments on ‘live’ nerves entail a period (t), from 0–240min, after injection of tracer into the sciatic nerve, during which the nerve fibers are exposed to tracer while the mouse is alive and anesthetized, followed by a period of ~30min during which the nerve is fixed, excised, rinsed, teased and mounted for examination. Our evidence from studies of fixed nerves is that aldehyde fixation does not ‘freeze’ the tracer in place; i.e. the tracer is still able to diffuse during the 30 min after fixation. Thus, the total time (T) for diffusion approximates t + 30min.

Statistical analysis

Statistical significance was determined with the Student t-test using Microsoft Excel and Statistical Package for the Social Sciences, SPSS. A p value of less than 0.05 was considered significant. A two-tailed t-test was used in all cases except for comparing dextran diffusion over time, where we hypothesized an increase in penetration with time, making the one-tailed t-test the appropriate statistical tool.

Diffusion calculations

Calculation of root mean square diffusion distances was based on the relationship: $x^2 = 2Dt$. Values for diffusion coefficient in brain (D*) in cm^2/sec were calculated from diffusion coefficients in dilute agarose (D) divided by the square of tortuosity (λ) derived from studies of normoxic rat neocortex in vivo (Sykova and Nicholson, 2008). The values used in our calculations are:

$D^* = 5.36 \times 10^{-7}$ 3K dextran
$D^* = 0.648 \times 10^{-7}$ 70K dextran

Time (t) was expressed in seconds.

To estimate distances diffused at times between those actually measured (Table 2), we multiplied distance measured at the nearest earlier time point by the square root of the ratio of the respective times.

Results

Dextran tracer penetration of paranodes in live nerve fibers

After tracer is injected into the sciatic nerve, it first appears at the node of Ranvier as a fluorescent slit perpendicular to the axonal axis (arrow, Fig. 1A–C). The 3K tracer (green) is usually washed out of the nodal slit during the rinse steps, but the 70K (red) tracer often persists at the node and also along the outer surface of the fiber (Fig. 1E and F). The tracer then penetrates into the fiber on both sides of the nodal slit more or less symmetrically forming a ‘bar’ whose length is indicated by the horizontal line in Fig. 1E and H. The extent of penetration varies at any given time point, but by 1.5hr, on average, the abnodal ends of the 3K paranodal bar have split into two tines (arrows, Fig. 1F), which then extend beyond into the internode (Fig. 1G–I), forming ‘hairpin-like’ configurations (Mierzwa and Rosenbluth, 2006). In all cases, superimposition of interference contrast and fluorescence images shows that tracer extending into the internodal domain still lies within the confines of the fiber, separated from the outermost surface by a narrow, non-fluorescent band (Fig. 1F and I).

The appearance of the dextran labeled fibers is variable in the paranodal region. Especially in larger fibers, the margin of the paranodal fluorescence is often ill-defined, and in focal regions it may give rise to radial or oblique extensions. PNS paranodes are well known to display regions in which clusters of terminal loops do not reach the axon surface. At these sites, the periaxonal space widens focally, thus creating periaxonal lacunae in which the tracers can pool, extending barb-like from the axon surface.

Even though the tracers may not cleanly delineate the paranode because of such irregularities, what is striking is that they penetrate rather symmetrically in both abnodal directions from the node. If the spread of tracer resulted from damage to a paranode, it is not likely that both paranodes would be so consistently and so equally damaged as to produce such a multiplicity of double ‘hairpin’configurations around nodes.

To determine the location of the tracers within the fiber, confocal stacks of longitudinally oriented images were rotated electronically to provide end-on views of the nerve fibers. In the Z stack shown in Fig 1P, a green fluorescent ring surrounds a dark core. That ring is in turn surrounded by a thick dark ring, and external to that, a faint thin red ring. We interpret these images as representing the axon (dark core) surrounded by 3K tracer in the periaxonal space (green ring), surrounded by compact myelin (dark ring), surrounded by 70K tracer outside the fiber, probably bound to its basal lamina (thin red ring). The ‘hairpin-like’ fluorescence seen in longitudinal images presumably arises from the green circumferential ring, which when viewed from above results in superimposition of fluorophores near the sides of the ring to a much greater extent than in the en face view. These images thus correspond to the appearance of a transilluminated empty green bottle, whose edges appear more heavily pigmented even though the glass is of uniform thickness. In the paranodal

region, where the axon is much narrower, neither confocal Z stacks nor single-slice orthogonal views are able to resolve the axon per se, presumably because of flare from fluorophores in the surrounding periaxonal space.

The average longitudinal extent of tracer penetration into live fibers increases with time (Table 1 and supplementary Fig. S1), progressing from the nodal slit to the paranodal ‘bar’ and finally the internodal 'hairpins'. The mean measured distances for dextran movement when the tissue was fixed immediately after tracer injection (the 0+30 time point) show the extent of tracer penetration during the 30min processing of the tissue. If these “tare” values (~1μm for the 3K tracer and ~0.4μm for the 70K tracer) are subtracted from the total distances recorded at later time points, the remainder represents movement only during the period when the nerves were alive.

Dextran penetration of paranodes in fixed fibers

Equivalent results were obtained fibers that had been fixed in a mixture of formaldehyde and glutaraldehyde, excised and soaked in 3K or 70K tracer labeled with fluorescein only. (Rhodamine B was not used in order to avoid confusion with glutaraldehyde autofluorescence.) The appearance of the 3K tracer images (Fig. 1 J–L) and 70K tracer images (Fig. 1 M–O), all correspond to what is seen after injection of the tracers into live nerves in situ. Here too, the paranodal ‘bar’ (horizontal line, Fig 1K and N) widens in a ‘shoulder’ region (arrows, Fig. 1K and N) and then forms internodal ‘hairpins’ (arrows, Fig. 1O) that can clearly be seen to lie within the outer margins of the fibers when the fluorescence and interference contrast images are superimposed. For comparable times of exposure to tracer, the glutaraldehyde/formaldehyde-fixed nerves show penetration to about the same extent as that seen in live unfixed fibers (Table 2). Since tracer penetration is observed in both live and fixed fibers, spread of the tracer cannot depend on endocytosis or intracellular transport or other energy-dependent cellular processes. The simplest mechanism to account for our results is, therefore, passive diffusion of these relatively inert tracers in both fixed and live nerve fibers.

Proportion of fibers showing paranodal penetration

In live-injected and in fixed sciatic nerves, both 3K and 70K dextrans show measurable penetration into some of the paranodes ('hits') at each time point studied. The number of paranodes penetrated in each coverslip studied is, however, very different for the respective tracers. As shown in Table S2, the 3K tracer penetrates more than 20X as many paranodes as the 70K tracer does in fixed nerves. In live-injected fibers, the difference is smaller, but the trend is similar.

Dextran tracer penetration of Schmidt-Lanterman clefts

In live-injected nerves, most fibers show no penetration of tracers except, as described above, via the paranodal region. However, occasional fibers (Fig. 2A–C) show penetration in internodal regions in a configuration consistent with movement through conical Schmidt-Lanterman clefts extending obliquely across the sheath on either side. The same fiber often shows multiple clefts along its length even though surrounded by other fibers that show none. In the example illustrated in Fig. 2B, the 3K tracer (green) extends across the full thickness of the myelin sheath into the periaxonal space and then spreads in both directions along the surface of the axon. The red 70K tracer (Fig. 2A) fills the cleft but does not spread within the periaxonal space.

In nerves soaked in the tracers *after* fixation, Schmidt-Lanterman clefts (arrow, Fig. 2D) also show dextran penetration equivalent to that seen in live nerves (Fig. 2E–F). Thus, here

too, the penetration cannot be attributed to endocytosis or any other energy-dependent process and therefore must occur by passive diffusion.

Distance penetrated by tracers

Calculation of diffusion distances, based on the sizes of the tracers and the diffusion coefficients obtained from prior studies of tracer spread in live brain (Sykova and Nicholson, 2008), show that the 3K tracer would be expected to move 440μm in 30min. This figure, based on root mean square calculations, depends on detection sensitivity, tortuosity and other factors and is, therefore, an approximation. Nevertheless, the distances actually seen in live and fixed preparations (0.9 and 2.2μm) were not even close to those calculated, differing, rather, by more than two orders of magnitude. Similarly, the 70K tracer would be expected to spread 324μm in 135min but was seen to penetrate only 4.4μm, again nearly two orders of magnitude less. Thus the average measured distances were far below those predicted.

Tables 1 and 2 show average observed distances of tracer movement at various time points in live and fixed fibers respectively. In all cases, there is a marked discrepancy between calculated diffusion distances and the penetration actually seen. This could reflect impeded diffusion due to friction between the tracer and the walls of the diffusion pathway, an effect that should be greater for the larger tracer. However, the apparent slowing of diffusion was comparable for both of the tracers used, despite the difference in their size. The discrepancy could also reflect increased viscosity of the fluid in the diffusion pathway. But in the fixed nerves the composition of the tissue spaces is undoubtedly different from that in the living nerve; yet the observed movement was comparable in the live and fixed nerves. In view of these considerations, the simplest explanation for our observations is that the diffusion pathway within the nerve fibers is much longer than it appears to be.

Pathways through the paranode (Fig. 3)

Extracellular spread of the tracers symmetrically within the nerve fiber on either side of the node could take place through the paranode as follows:

Pathway 1. Dextran could diffuse axially within the 2–4nm paranodal junctional gap right *across* the transverse bands to reach the juxtaparanode and then beyond within the internodal periaxonal space. The pathway through the paranode in this case would consist of a cylindrical space ~2–4nm in thickness and several μm long, corresponding to the length of the paranode.

Pathway 2. Dextran could diffuse *along* the spaces between the ridge-like transverse bands, as suggested by Hirano and Dembitzer (1969). In this case, since the transverse bands are oriented obliquely with respect to fiber axis, the tracers instead of moving axially would move through the PNJ at a markedly oblique angle, approximating, in mice, 8 degrees off the plane transverse to the axonal axis (Rosenbluth, 2009). The length of this path would be inversely proportional to the sine of that angle or ~ 7-fold longer than pathway 1, which passes axially across the PNJ.

As indicated above, however, neither of these pathways can account for the relatively short apparent distance moved by the tracers, resulting in a disparity between measured and calculated diffusion distances approximating two orders of magnitude. Moreover, both of these paths are only 2–4nm in width. Although the 3K tracer is ~2.6nm in diameter, i.e., comparable to the apparent width of the paranodal periaxonal space, the 70K tracer, ~12–16nm in diameter, is larger than that by several fold. For this reason passive diffusion through the paranodal periaxonal space, either axially (pathway 1) or obliquely (pathway 2),

seems impossible for the 70K tracer and unlikely for the 3K tracer. In order to account for the observed distances, we must therefore postulate a different route.

The third pathway

Myelin is well known to form by spiral wrapping of the myelin-forming cell around the axon. The resulting PNJs at the edges of each myelin segment are, accordingly, helical in form (Robertson, 1959). Thus, each paranodal loop seen in longitudinal sections is in fact part of a single continuous cytoplasmic column sectioned multiple times as it winds around the axonal circumference. Adjacent loops, spaced ~0.1μm apart in the axial direction, appose each other closely and indeed form tight junctions with each other, but near the axonal surface their plasma membranes curve away from each other resulting in the formation of a small extracellular space, roughly triangular in profile, between adjacent loops close to their junction with the axolemma. Just as the loops themselves are part of a continuous helical cytoplasmic column, the triangular spaces between them form a continuous extracellular channel parallel to the cytoplasmic column (illustrated in Fig. 3), extending helically with a pitch of ~0.1μm from the node of Ranvier through the paranode to the juxtaparanodal periaxonal space. This narrow channel is significantly wider than the paranodal junctional cleft and thus represents a pathway through the paranode of sufficient caliber to accommodate the dextran tracers we have been using. This pathway is, however, much longer than the length of the paranode.

Specifically, each turn of this extracellular helix is roughly as long as the axonal circumference, and the number of turns of the helix depends on the number of myelin lamella that form terminal loops against the axon. Thus, if an axon were 10μm in diameter, narrowing to 5μm in the paranodal region, with a 5μm-long paranode comprised of 50 paranodal loops having a helical pitch of ~0.1μm, the length of the helix from the node of Ranvier to the juxtaparanodal region would approximate $5\pi \times 50$, or ~785μm. In contrast, pathway 1 passing axially through the paranodal periaxonal space would be only ~5μm long, and pathway 2, passing obliquely along the transverse bands, would be only ~35μm long. A fluorescent particle following the third pathway would have to move nearly 800μm helically in order to advance 5μm in the axial direction. Beyond the paranode, the particle would move within the internodal periaxonal space directly in the axial direction at a much greater apparent rate.

Comparing the calculated distances diffused through these three pathways with the apparent distances moved in the axial direction (Tables 1 and 2), it is clear that only movement through the third pathway can account for the observed progression of the dextran tracers through the paranode; extracellular pathways1 and 2 are far too short to account for the data, as the intracellular diffusion path through the axon would be in the event that some tracer had crossed the nodal axolemma. Correspondingly, the calculated diffusion *time* for the 3K tracer to traverse the paranode axially is on the order of seconds in pathways 1(0.23s) and 2(12s), but the observed time is on the order of hours (1.5hrs), again consistent with the movement of dextran through the circuitous pathway 3 (calculated time to traverse the 5μm paranode = ~95min).

That the 70K tracer follows the helical pathway is expected, as discussed above, considering the size of this tracer, which is several times larger than the width of the PNJ cleft. Surprisingly, the diffusion calculations indicate that the 3K tracer also follows this pathway. Even in a mouse mutant (‘CST-null’) characterized by a gross deficiency of transverse bands, the permeability of the PNJ to 3K dextran is comparable to that in control mice. Thus, here too the tracer apparently still follows pathway 3 through the paranode rather than pathways 1 or 2 through the junctional cleft (Shroff et al., 2009).

Diffusion beyond the paranode is complicated by the fact that the cross-sectional area of the internodal periaxonal space is much larger than that of the helical pathway 3. Specifically, if the cross-section of pathway 3 approximates an equilateral triangle 20nm on each side, the area of the triangle would approximate 170nm^2. Pathway 3 would empty into the periaxonal space of the juxtaparanode, whose diameter, using the example above, would then quickly widen to 10μm in the internodal region. The cross sectional area of the internodal periaxonal space would thus approximate the circumference of the axon multiplied by the width of the space, i.e., $10\pi\times10^3$ nm × 10–20nm, or ~300,000–600,000nm^2, a difference of ~1800–3500 fold! Tracer following the third pathway would thus become markedly diluted, and as the tracer continued to diffuse axially along the internode, it would be replenished at a very limited rate via the efflux from pathway 3. For these reasons, tracer moving beyond the paranode may rapidly diminish in concentration below the level of detection, and measurements in this region may thus not be accurate. This probably accounts for the small apparent difference in 3K tracer penetration at 150 and 270min (supplementary Fig S1). Despite the dilution factor, the 3K tracer does, nevertheless, become visible in the juxtaparanode and in internodal 'hairpins' at a time consistent with diffusion through pathway 3 in the paranode.

Discussion

Functional significance of paranodal permeability

Penetration of the paranodal junction by water-soluble molecules provides a means by which a variety of biologically important materials can reach the internodal axon. In view of the high lipid content of myelin, aqueous solutes cannot diffuse across the myelin sheath to the periaxonal space. Here we provide evidence for a paranodal pathway bypassing this barrier and, to a limited degree, a pathway through Schmidt-Lanterman clefts. These paths would permit such materials as glucose, other water soluble nutrients and hormones such as thyroxin and insulin to diffuse into the internodal periaxonal space forming a reservoir there in immediate contact with the axolemma all along its length. These paths also represent routes for diffusion of water-soluble metabolites away from the axon.

Our results are relevant also to human diseases associated with penetration of peripheral nerve myelin sheaths by antibodies or toxic agents. Guillain-Barre syndrome, an autoimmune disease in which components of myelin and/or axons are damaged by a cellular or humoral attack, may depend on penetration of the PNJ by antibodies or such immune effectors as granzyme and complememt components, as well as by cell processes. Our results are relevant also to acquired neuromyotonia which has been shown to result from autoantibodies to JP K+ channels (Kleopa et al, 2006). Similar mechanisms may operate in paraneoplastic neuropathies (Vincent, 2004). Our permeability data may be relevant as well to CNS diseases, such as multiple sclerosis and central paraneoplastic syndromes. Small fluorescent peptides have been shown to reach and bind to JP K+ channels in CNS explants (Devaux and Gow, 2008). The permeability of living CNS paranodal junctions to larger macromolecules, the size of antibodies, is not yet known, however.

Finally, demonstration of a patent pathway through the paranode opens up the prospect that under some circumstances enough current could follow that route to activate JP K+ channels and that the latter could reciprocally affect nodal excitability. These JP K+ channels have been a source of consternation because they are covered by the myelin sheath and apparently isolated from the node and thus have no obvious role in signal propagation. Yet the nerve cells make a considerable investment in producing them and transporting them to their ultimate location, and their absence does have functional consequences (Chiu et al., 1999). The pathway through the paranode demonstrated here renders them accessible to a limited and perhaps variable degree, depending on the physiologic state (Moran and Mateu, 1983)

or developmental state (Vabnick et al., 1999) of the nerve and any pathologic processes operating, and thus represents a route by which these apparently isolated channels may affect nodal properties and behavior. This route for current flow, which we show here is patent in living nerve fibers, is in addition to other possible extracellular routes for current flow, e.g., pathways 1 and 2 through the PNJ and the extracellular spaces in Schmidt-Lanterman clefts, whose conductances are unknown.

The evidence that JP K+ channels affect nodal behavior in normal CNS myelinated fibers, particularly those of small-caliber (Devaux and Gow, 2008), is consistent with our suggestion that pathway 3 might serve as a route through which K+ channel activity affects nodal behavior. The length of that path depends on the number of helical wraps made by the paranodal edges of the sheath, which in turn depends on the number of myelin lamellae. Thus, in the example of the PNS fiber referred to earlier with 5μm paranodes and 50 lamellae of myelin, pathway 3 would be very long--785μm. In a CNS fiber with 1μm diameter paranodes and 15 myelin lamellae, pathway 3 would be only 47μm, a 16-fold reduction! Thus in small-caliber fibers, JP K+ channels are connected to the node by a much shorter and correspondingly less resistive pathway than that of large-caliber fibers and are therefore more likely to exert effects on nodal behavior. To what extent the results of the in vitro studies cited above reflect the behavior of small-caliber myelinated fibers in vivo is uncertain.

Evidence that access to and from JP K+ channels affects saltatory conduction also comes from studies of dysmyelinating mutants lacking transverse bands, e.g. the Caspr-null mouse, which display a pronounced reduction in PNS conduction velocity (Bhat et al., 2001). In the absence of transverse bands, these channels are mislocated to the paranode, and the path interconnecting them with the node is thus greatly shortened. In contrast, dysmyelinating mutants whose transverse bands are preserved show normal segregation of K+ channels to the juxtaparanode, and in those, normal conduction velocity is preserved (Mierzwa et al., 2010).

Schmidt-Lanterman clefts

These structures have been regarded as possibly artifacts of specimen preparation or ‘shearing defects’ (Robertson, 1958), but studies of living nerve fibers in culture showed SL clefts to be present there too (Bunge et al., 1967). It has also been suggested that they are dynamic; i.e., they can translocate along the axon, or they can open and close (Hall and Williams, 1970).

In all cases, SL clefts are characterized by two features (Robertson, 1958; Hall and Williams, 1970): 1. a conical stack of myelin lamellae that lose their compaction over a short length; i.e. each ‘major dense line’, representing the fused cytoplasmic surfaces of the myelinating Schwann cell, splits to enclose cytoplasm, and 2. the external surfaces of the apposed Schwann cell membranes, which form the intraperiod (or intermediate) line, separate to create a larger aqueous gap ~10nm in width, which may expand even further under some circumstances, e.g. a hyposomotic environment. Circumferential microtubules have been described within the cytoplasmic component, and both adhesive and tight junctions have been described linking the component membrane pairs together (Hall and Williams, 1970).

Nodes of Ranvier, where the external contour of the nerve fiber changes dramatically, are readily identified by Hoffman interference contrast microscopy. SL clefts, in contrast, where the axon diameter is unchanged, are much more difficult to recognize and could be identified only infrequently in the Hoffman mode in our teased preparations. Hence,

although we know that tracer was able to penetrate some, as shown in Fig. 2, we cannot say what proportion of the total that represents.

Biochemically, myelin-associated glycoprotein (MAG) is associated with regions of cytoplasm-containing myelin membranes, including the SL clefts (Schober et al., 1981; Trapp, 1990) along with Nectin-like proteins (Maurel et al., 2007). A circumferential strip of axolemma containing Caspr, flanked by shaker-type K+ channels, faces the innermost extent of each SLC cone (Arroyo et al., 1999). Considering the complexity of the membrane differentiations associated with SLCs, it is difficult to imagine that this constellation of structures could be rapidly mobile within the myelin sheath. However, in the absence of 'spacers', comparable to transverse bands, to maintain a constant separation between the apposed external surfaces of the SLC membranes, variations in gap width depending on functional state or environment might well occur and might account for the variability we see in penetration of SLCs by dextran tracers. Thus, SLCs may be subject to much greater fluctuation in permeability and conductance than paranodal junctions are.

Summary and conclusions

We show that 3K and 70K dextran tracers are able to penetrate through the paranodes of myelinated nerve fibers of mouse sciatic nerve both in life and after fixation. Thus, a patent pathway through the paranode that can accommodate molecules as large as ~12–16nm in diameter exists in living fibers and is preserved after fixation. Since movement of the tracers takes place at about the same rate in live and fixed nerves; the movement cannot depend on endocytosis or other metabolism-dependent processes and is most simply explained by passive diffusion.

The rate of movement of both 3K and 70K dextrans through the paranodes is consistent with movement through an elongated pathway, which we propose consists of the helical channel we refer to as pathway 3. This channel passes between successive terminal loops of the paranodal junction beginning at the perinodal space and ending under the myelin sheath at the juxtaparanodal periaxonal space.

We propose also that this pathway serves as a route for movement of water soluble materials to and from the internodal periaxonal space and that it may serve as a pathway for current flow to and from juxtaparanodal potassium channels.

Supplementary Material

Refer to Web version on PubMed Central for supplementary material.

Acknowledgments

The authors are indebted to Drs. Charles Nicholson, Sabina Hrabetova and Robert Thorne for invaluable discussions, to Dr. R. Schiff for help with photography and measurements and to Chris Petzold for expert technical assistance. This work was supported by research grants from the NIH (NS37475) and the National Multiple Sclerosis Society (RG3618).

References

Arroyo EJ, Xu YT, Zhou L, Messing A, Peles E, Chiu SY, Scherer SS. Myelinating Schwann cells determine the internodal localization of Kv1.1, Kv1.2, Kvbeta2, and Caspr. J Neurocytol. 1999; 28:333–347. [PubMed: 10739575]

Bhat MA, Rios JC, Lu Y, Garcia-Fresco GP, Ching W, St Martin M, Li J, Einheber S, Chesler M, Rosenbluth J, Salzer JL, Bellen HJ. Axon-glia interactions and the domain organization of

myelinated fibers require neurexin IV/Caspr/paranodin. Neuron. 2001 May.30:369–383. 2001. [PubMed: 11395000]

Brismar T. Specific permeability properties of demyelinated rat nerve fibres. Acta Physiol Scand. 1981; 113:167–176. [PubMed: 7315447]

Bunge MB, Bunge RP, Peterson ER. Murray MRA light and electron microscope study of long-term organized cultures of rat dorsal root ganglia. J Cell Biol. 1967; 32:439–466. [PubMed: 10976233]

Chiu SY, Ritchie JM. Potassium channels in nodal and internodal axonal membrane of mammalian myelinated fibres. Nature. 1980; 284:170–171. [PubMed: 6244497]

Chiu SY, Zhou L, Zhang C-L, Messing A. Analysis of potassium channel functions in mammalian axons by gene knockouts. J Neurocytol. 1999; 28:349–364. [PubMed: 10739576]

Devaux J, Gow A. Tight junctions potentiate the insulative properties of small CNS myelinated axons. J Cell Biol. 2008; 183:909–921. [PubMed: 19047465]

Feder N. Microperoxidase. An ultrastructural tracer of low molecular weight. J Cell Biol. 1971; 51:339–343. [PubMed: 4106859]

Hall SM, Williams PL. Studies on the "incisures" of Schmidt and Lanterman. J Cell Sci. 1970; 6:767–791. [PubMed: 5452094]

Hirano A, Dembitzer HM. The transverse bands as a means of access to the periaxonal space of the central myelinated fibre. J Ultrastruct Res. 1969; 28:141–149. [PubMed: 5791690]

Huxley AF, Staempfli R. Evidence for saltatory conduction in peripheral myelinated nerve-fibers. J. Physiol. 1949; 108:315–339.

Kleopa KA, Elman LB, Lang B, Vincent A, Scherer SS. Neuromyotonia and limbic encephalitis sera target mature Shaker-type K+ channels: subunit specificity correlates with clinical manifestations. Brain. 2006; 129:1570–1584. [PubMed: 16613892]

Kocsis JD, Waxman SG. Absence of potassium conductance in central myelinated axons. Nature. 1980; 287:348–349. [PubMed: 7421994]

Maurel P, Einheber S, Galinska J, Thaker P, Lam I, Rubin MB, Scherer SS, Murakami Y, Gutmann DH, Salzer JL. Nectin-like proteins mediate axon Schwann cell interactions along the internode and are essential for myelination. J Cell Biol. 2007; 178:861–874. [PubMed: 17724124]

Mierzwa AJ, Arevalo JC, Schiff R, Chao MV, Rosenbluth J. Role of transverse bands in maintaining paranodal structure and axolemmal domain organization in myelinated nerve fibers: effect on longevity in dysmyelinated mutant mice. J Comp Neurol. 2010; 518:2841–2853. 2010. [PubMed: 20506478]

Mierzwa AJ, Rosenbluth J. Lateral permeability of the paranodal junction in myelinated nerve fibers. Soc Neurosci. 2006 Poster 638.6/L3, annual meeting.

Morán O, Mateu L. Loosening of paranodal myelin by repetitive propagation of action potentials. Nature. 1983; 304:344–345. [PubMed: 6877354]

Robertson JD. The Ultrastructure of Schmidt-Lanterman clefts and related shearing defects of the myelin sheath. J Biophys Biochem Cytol. 1958; 4:39–46. [PubMed: 13502426]

Robertson JD. Preliminary observations on the ultrastructure of nodes of Ranvier. Z Zellforsch. 1959; 50:553–560.

Rosenbluth J. Multiple functions of the paranodal junction of myelinated nerve fibers. J. Neurosci. Res. 2009; 87:3250–3258. [PubMed: 19224642]

Schober R, Itoyama Y, Sternberger NH, Trapp BD, Richardson EP, Asbury AK, Quarles RH, Webster HD. Immunocytochemical study of P0 glycoprotein, P1 and P2 basic proteins, and myelin-associated glycoprotein (MAG) in lesions of idiopathic polyneuritis. Neuropathol Appl Neurobiol. 1981; 7:421–434. [PubMed: 6173794]

Sherratt RM, Bostock H, Sears TA. Effects of 4-aminopyridine on normal and demyelinated mammalian nerve fibres. Nature. 1980; 283:570–572. [PubMed: 7354839]

Shroff S, Mierzwa A, Rosenbluth J. Permeability of the paranodal junction to dextran tracers in CST-null and wild-type sciatic nerves. Soc Neurosci. 2009 Poster 724.14/G2, annual meeting.

Syková E, Nicholson C. Diffusion in Brain Extracellular Space. Physiol. Rev. 2008; 88:1277–1340. [PubMed: 18923183]

Tasaki I. The electro-saltatory ransmission of the nerve impulse and the effect of narcosis on the nerve fiber. Am.J Physiol. 1939; 127:211–227.

Trapp, BD. The myelin-associated glycoprotein: location and potential functions. In: Colman, D.; Duncan, I.; Skoff, R., editors. Myelination and Dysmyelination. Vol. vol. 605. New York: The New York Academy of Sciences; 1990. p. 29-43.

Vabnick I, Trimmer JS, Schwarz TL, Levinson SR, Risal D, Shrager P. Dynamic potassium channel distributions during axonal development prevent aberrant firing patterns. J Neurosci. 1999; 19:747–758. [PubMed: 9880595]

Vincent A. Antibody-mediated disorders of neuromuscular transmission. Suppl Clin Neurophysiol. 2004; 57:147–158. [PubMed: 16106615]

Wang H, Kunkel DD, Martin TM, Schwartzkroin PA, Tempel BL. Heteromultimeric K+ channels in terminal and juxtaparanodal regions of axons. Nature. 1993; 365:75–79. [PubMed: 8361541]

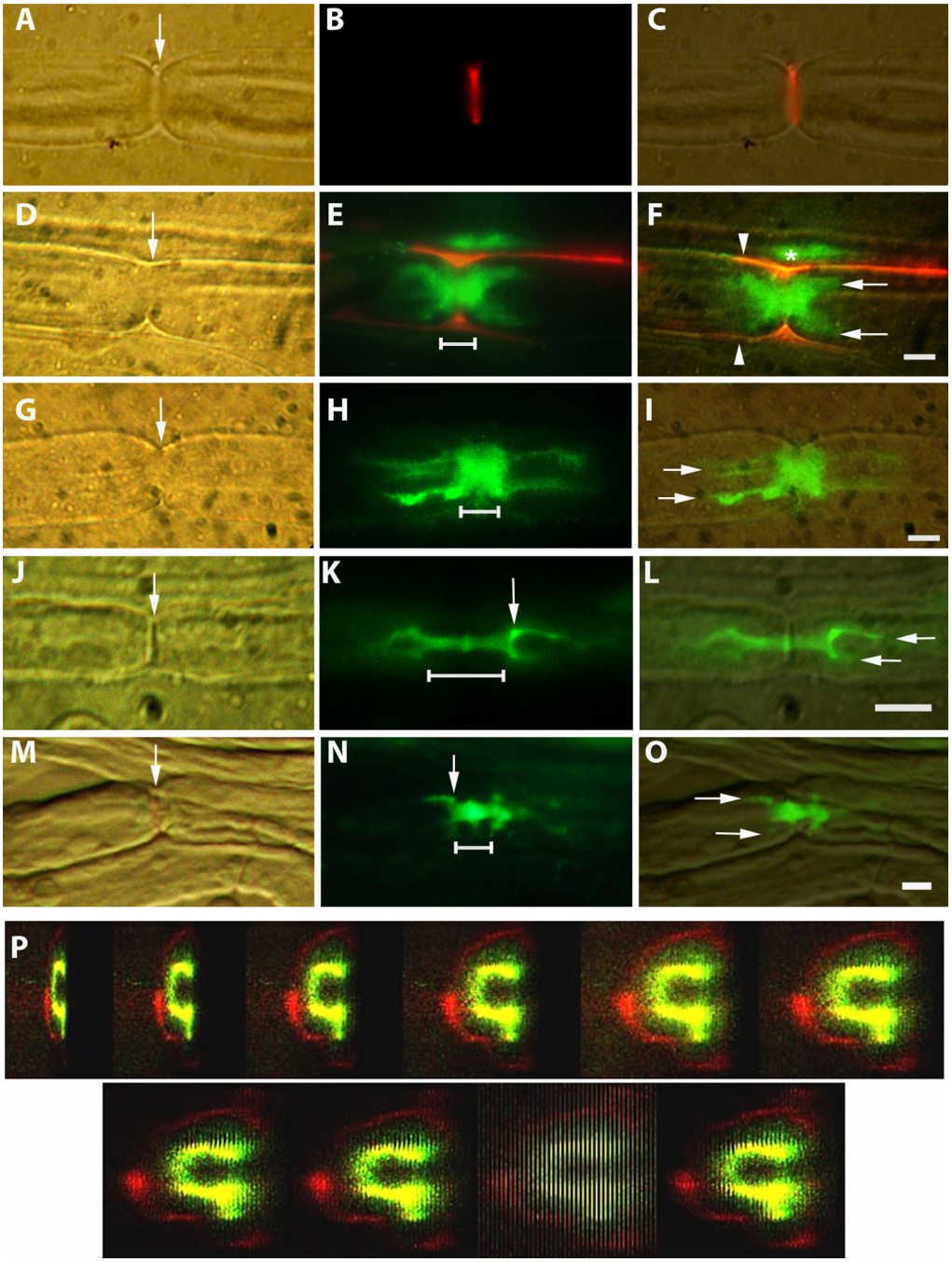

Fig. 1.

A–O., Hoffman, fluorescence and merged images showing penetration of dextran tracers into node/paranode regions of sciatic nerve myelinated fibers. Scale bars = 5microns. The node of Ranvier is indicated by arrows in A, D, G, J and M. The linear extent of 'paranodal bars' is indicated by horizontal lines in E, H, K and N.

A–C. Live injection. 70K tracer (red) fills the nodal slit (arrow).

D–F. Live injection. 70K tracer (red) outlines a nerve fiber (E and F). Between the red outlines (arrowheads, F), 3K tracer (green) has penetrated from the node into the fiber symmetrically forming a thick paranodal 'bar' just beginning to give rise to the tines

(arrows, F) of ‘hairpins’ at both ends. Some 3K tracer above this fiber (*) has been trapped between it and a 2nd fiber whose outline is visible above.
G–I. Live injection. 3K tracer (green) forms a paranodal ‘bar’, which widens to form conspicuous ‘hairpins’ (arrows) symmetrically on both sides of the node.
J–L. Fixed nerve exposed to 3K tracer (green), which forms a narrow paranodal ‘bar’ (line, K) that is slightly wider just at the node. At both ends, the bar widens in a ‘shoulder’ region (arrow, K), where it forms ‘hairpins’ that extend into the intermodal periaxonal space.
M–O. Fixed nerve exposed to 70K tracer (green), which forms a short ‘bar’ (line, N) that gives rise to square ‘shoulder’ regions (arrow, N) at each end and the beginnings of ‘hairpin’ tines (arrows, O).
P. Live injection. Confocal Z stack rotated to show dark core (internodal axon), surrounded by 3K dextran (green) in the periaxonal space. That in turn is surrounded by a dark ring (compact myelin) and outside of that a thin red ring (70K dextran) along the outside of the fiber. The 9th image in the series shows the confocal slices end on.

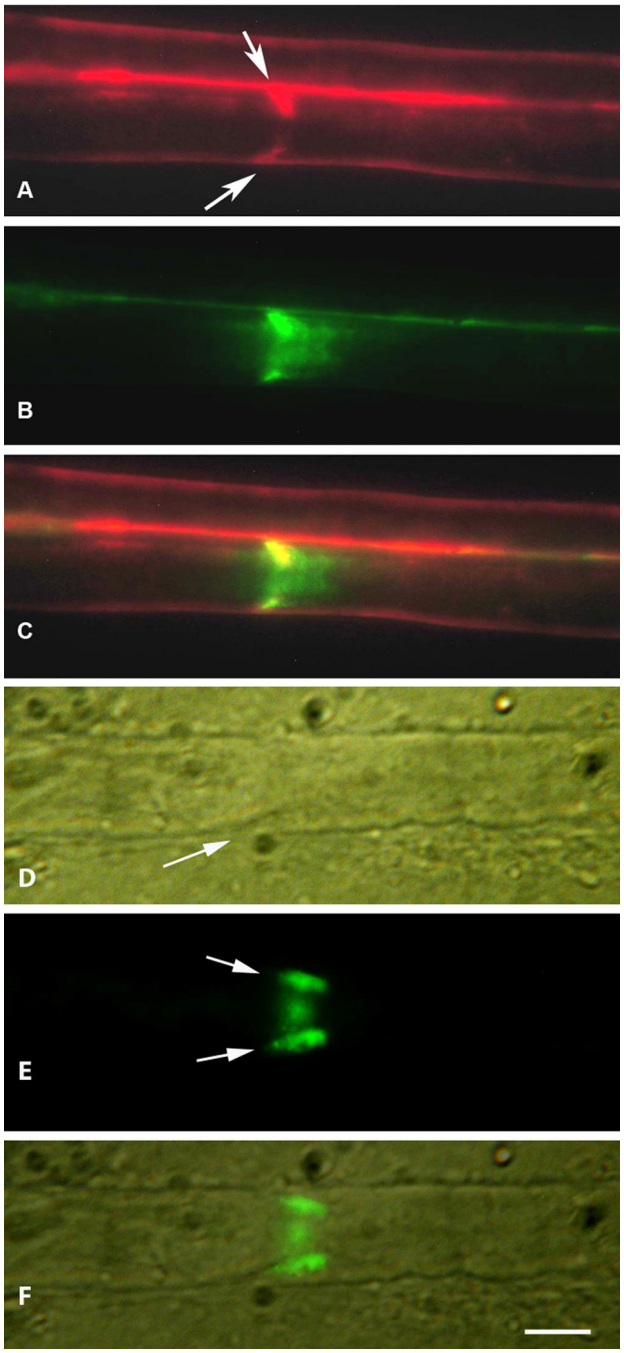

Fig. 2.

A–C. Schmidt-Lanterman cleft (live injection). Both tracers 70K (red) and 3K (green) outline the outer surface of the fiber, and (at arrows) both extend obliquely from the fiber surface toward the axon. The 3K tracer then spreads longitudinally along the axon in both directions (B). The 70K tracer (A) does not extend beyond the inner end of the cleft. C. Merged A and B images. In A and C, the red outline of a second fiber is visible above the outline of the first.

D–F. Schmidt Lanterman cleft in fixed fiber exposed to 70K dextran (green) for 4hr. Arrows in E show the tracer extending obliquely into the cleft (arrow in D) toward the axon from

both sides of the fiber and visible also in the en face view between. F. Merged D and E images.

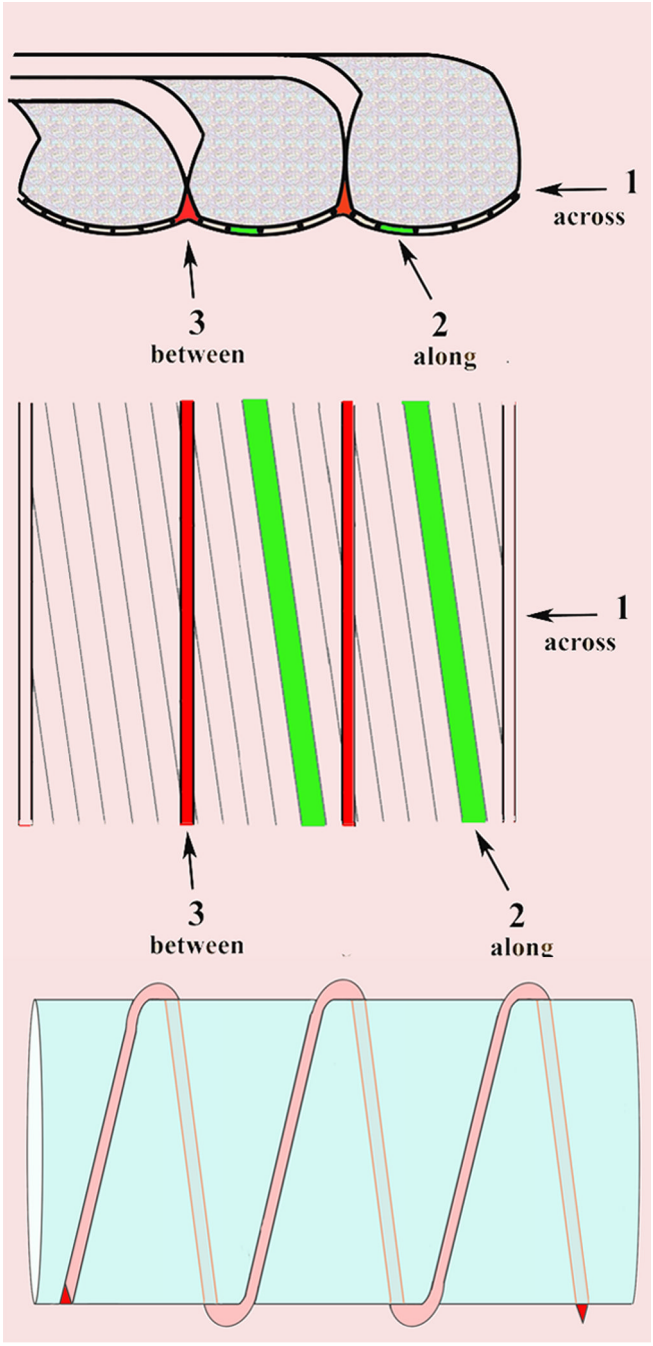

Fig. 3.

Schematic representations of possible pathways of diffusion

Top. Side view of paranodal loops.

Middle. Tangential view. Pathway 1 goes through the junctional cleft *across* the transverse bands. Pathway 2 also goes through the junctional cleft but passes *along* the transverse bands at ~8 degrees from transverse. Pathway 3 does not go through the junctional cleft but passes *between* paranodal loops.

Bottom. Longitudinal view of pathway 3 winding helically around an axon.

Table 1

Dextran penetration (µm) in LIVE-injected fibers

Calculated and measured dextran tracer penetration in live fibers. Tracer penetration through different pathways in a fiber assumed to have a paranode 5µm in diameter and 5µm long with transverse bands oriented at 8 degrees to the transverse plane and with paranodal loops spaced at 0.1µm intervals. Average measured penetration approximates calculated penetration through pathway 3 but differs from that through pathways 1 or 2 by ~ two orders of magnitude. Each 'Calculated' value represents the axial distance (µm) moved on one side of a node in the PN plus distance in the IN. Each 'Measured' value represents apparent axial extent of tracer penetration (± SD). n, number of paranodes measured.

		Pathways				
Tracer	**Time (min)**	**1**	**2**	**3**		
	Total (live+prep)	**Calculated**			**Measured**	**n**
3K	30 (0+30)	440	409	2.8	**1.0 ± 0.9**	14
	60 (30+30)	621	590	4.0	**3.2 ± 2.8**	16
	90 (60+30)	762	731	4.9	**5.4 ± 4.2**	45
70K	30 (0+30)	153	122	1.0	**0.4 ± 0.3**	14
	60 (30+30)	216	185	1.4	**1.3 ± 0.9**	16
	90 (60+30)	264	233	1.7	**1.8 ± 1.3**	45
	150 (120+30)	341	310	2.2	**5.9 ± 2.8**	24

Table 2

Dextran penetration (μm) in FIXED fibers

Calculated and measured dextran penetration in fixed fibers. The expected tracer penetration through different pathways in a fiber was calculated as in Table 1. Here too, average measured penetration at all time points approximates calculated penetration through pathway 3, but differs from that through pathways 1 and 2 by ~ two orders of magnitude. For comparison with live fibers, diffusion for corresponding time points has been estimated from the measured values. n, number of paranodes measured.

Tracer	Time (min)	Pathways 1	2	3	Measured	n	Estimated
		Calculated					
3K	30	440	409	2.8	**2.2 ± 1.4**	15	
	45	540	509	3.4	**2.6 ± 1.5**	35	
	60	621	590	4.0			**3.0**
	75	650	619	4.1	**5.3 ± 2.8**	210	
70K	135	324	293	2.1	**4.4 ± 2.6**	207	
	150	342	311	2.2			**4.6**